Dyes and Pigments 103 (2014) 202–213

Contents lists available at ScienceDirect

Dyes and Pigments

journal homepage: www.elsevier.com/locate/dyepig

# Ground and excited state properties of alizarin and its isomers

Justyna Mech [a,1], Maria A. Grela [b], Konrad Szaciłowski [a,c,*]

[a] AGH University of Science and Technology, Faculty of Non-Ferrous Metals, Al. A. Mickiewicza 30, PL-30059 Krakow, Poland
[b] Departamento de Química, Facultad de Ciencias Exactas y Naturales, Universidad Nacional de Mar del Plata, B7602AYL Mar del Plata, Buenos Aires, Argentina
[c] Faculty of Chemistry, Jagiellonian University, Ingardena 3, PL-30060 Krakow, Poland

ARTICLE INFO

*Article history:*
Received 25 September 2013
Received in revised form
29 November 2013
Accepted 7 December 2013
Available online 17 December 2013

Dedicated to professor Krzysztof Fitzner of the occasion of his 70th birthday.

*Keywords:*
Alizarin
Excited state
Reorganization
Density functional theory
Optical spectroscopy
Dihydroxyanthraquinone

ABSTRACT

Four different alizarin dyes are studied with optical, electrochemical and quantum-chemical techniques. Despite structural similarities they show marked differences regarding both ground and excited state properties. All these dyes are characterized with strong HOMO–LUMO transitions of internal charge transfer character. These transitions, however, show different reorganization energies due to involvement of intramolecular proton transfer processes. Differences in charge redistribution upon excitation may lead to different photochemical reactivity of these species and also to different behavior in dye-sensitized solar cells and other devices.



## 1. Introduction

Rapid development of photocatalysis [1], photovoltaics [2], and infochemistry [3] relies on novel materials with precisely tailored properties. Furthermore, the synthesis of these materials should be cheap and environmentally-friendly. A large variety of organic chromophores, displaying desired properties can be used as semiconductor surface modifiers or exploited directly as functional materials in numerous applications. In particular, dihydroxyanthraquinones (DHAQs) constitute an interesting family of compounds. They are anthraquinone dyes bearing –OH and C=O moieties which may be used to anchor these dyes to semiconductor surfaces. Scheme 1 presents the most relevant structural isomers of DHAQs. These dyes are easily distinguishable by their color which varies from greenish yellow for anthrarufin, yellowish orange for alizarin, intense orange for chrysazin to dark red for quinizarin. Physical form of these dyes in the pure form also varies. Alizarin (C.I. 58000), quinizarin and anthrarufin are usually fine powders, whereas chrysazin occurs as well developed crystals. The variety of colors of the above species is a result of different electronic transitions and different type of electron delocalization manifolds within molecules. Despite structural similarities, dihydroxyanthraquinones present surprisingly different redox and spectral characteristics and thus find different applications.

The leading example of anthraquinone derivative used as a dye is alizarin, known as Turkish red or Mordant Red 11. The discovery of a synthetic method of alizarin fabrication in the second half of the 19th century revolutionized the textile industry. The British Army red coats serve as a good example of large scale production of colored fabrics. The affinity of alizarin towards the p-block (aluminum, tin, lead) and d-block (zinc, copper, cadmium, cobalt, nickel, iron, chromium, zircon, scandium) cations is well documented. Formation of strongly colored complexes (usually of low solubility in water) is commonly used for trace metal extraction and quantification [4–6]. Its ability of binding calcium makes alizarin useful in biochemical studies involving bone growth and osteoporosis, gene expression and tissue engineering [7–9]. It is also used in geology as a marker of calcium containing minerals [10] or in ore-mining industry as an organic foam depressant in the flotation

* Corresponding author. AGH University of Science and Technology, Faculty of Non-Ferrous Metals, Al. A. Mickiewicza 30, PL-30059 Krakow, Poland. Tel.: +48 12 617 29 31; fax: +48 12 633 23 16.
*E-mail addresses:* justyna.mech@agh.edu.pl (J. Mech), magrela@mdp.edu.ar (M.A. Grela), szacilow@agh.edu.pl (K. Szaciłowski).
[1] Tel.: +48 12 617 29 31; fax: +48 12 633 23 16.

0143-7208/$ – see front matter © 2013 Elsevier Ltd. All rights reserved.
http://dx.doi.org/10.1016/j.dyepig.2013.12.009

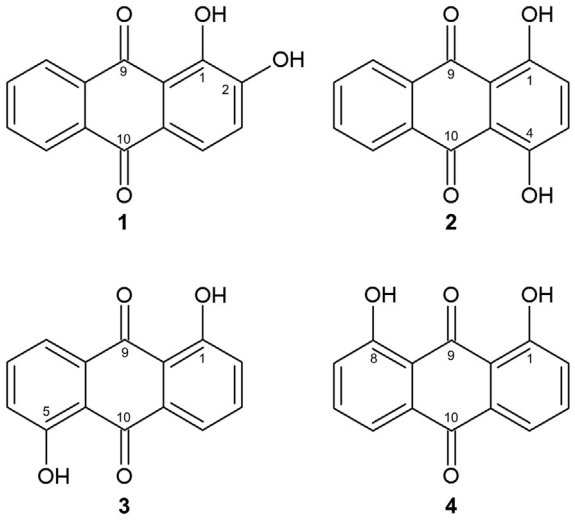


**Scheme 1.** Molecular structure of alizarin (**1**), quinizarin (**2**), anthrarufin (**3**) and chrysazin (**4**).

process [11]. It is also suitable in fluorimetric detection of boron compounds and fluoride anions [6,12–14]. 1,4-dihydroxyanthra quinone has received some attention as an anticancer drug [15]. It is used also as a fungicide and a pesticide. Furthermore, it finds niche applications as an additive in lubricants. Quinizarin forms fluorescent complexes with lithium, boron and aluminum which makes it useful for spectrofluorimetric detecting of these elements [16,17]. Anthrarufin was found to be active against Gram-positive bacteria, as well as it reduces damaging effects of dioxin [18]. Chrysazin (also known as danthron) has been widely used as a laxative till the eighties, when American manufacturers withdrew this compound from drug production because of carcinogenic risk for human. Chrysazin is also widely used in some metal ion determinations, *e.g.* lithium, magnesium, calcium, copper, lead, cadmium, zinc, nickel, manganese, iron, cobalt, palladium and platinum [19]. Photochemical reduction of some dihydroxyanthraquinones leads to the generation of semiquinone radical anions and a number of reactive oxygen species including singlet oxygen $O_2(^1\Delta_g)$ [20–23]. The anthraquinone derivatives also are commonly used in electrocatalytic processes, for example for reduction of molecular oxygen [24–26]. Alizarin and quinizarin naturally occur in the roots of the madder plant (*Rubia tinctorum*), anthrarufin is found in some species of fungi (*Aspergillus glaucus*, *Trichoderma sp.*) and bacteria (*Xenorhabdus sp.*), chrysazin can be extracted form dried leaves and stems of *Xyris semifuscata*, a plant harvested in Madagascar.

Even though those compounds have been known for centuries, mainly because of their coloring properties, their chemistry has recently received a lot of attention in relation to their use as $TiO_2$ surface modifiers [24,27–34]. Alizarin–$TiO_2$ couple becomes a model system for examining dynamics of the electron injection from the molecule to the semiconductor in the weak electronic coupling regime [29–33,35–38]. Alizarin is a good photosensitizer, and arouses great interest as a modifier in dye-sensitized solar cells. Recently some DHAQ dyes were involved in the synthesis of $TiO_2$-based materials for optoelectronic systems [27,28]. This class of photoactive materials reveals unusual photocurrent–voltage curves. Particularly, the $TiO_2$ electrodes modified with alizarin and alizarin complexone ligands show both anodic and cathodic photocurrents depending on the applied external potential. Anodic photocurrents are observed when an excited electron is transferred from the conduction band of the semiconductor towards the conducting support with the concomitant oxidation of the redox mediator present in the electrolyte. In contrary, cathodic photocurrents are generated when an electron from the conduction band (or from a sensitizer-based surface state) is transferred to the redox mediator present in the electrolyte. This phenomenon is called photoelectrochemical photocurrent switching effect (PEPS) [39,40]. Materials revealing PEPS have great potential in optoelectronics as they can be used for construction of optical switches, logic gates and other information processing devices [39–50]. The knowledge about ground and excited states of the aforementioned molecules is also relevant in photovoltaics and photocatalysis, where dyes are implemented in sophisticated structures often containing semiconductor or metal nanostructures. Information on adsorption properties of molecules and its ability for self-organization as well charge donating character is indispensable in designing efficient hybrid systems.

Previous works describe ionic forms [51], tautomerism [36,52] or photocatalytic properties [22] of dihydroxyanthraquinones. Recent reports also emphasize the role of geometry of the photosensitizer molecule on the mechanism and efficiency of photoinduced processes at the $TiO_2$ surface [24,27,53]. However, there are no comprehensive studies on spectroscopy and electrochemistry of the dihydroxyanthraquinone dyes which take into account the positional isomerism. The special emphasis is placed on possible forms of the dyes in the solid as well as in liquid phases (solutions). The present study involves four dihydroxyanthraquinone dyes (Scheme 1): alizarin (**1**), quinizarin (**2**), anthrarufin (**3**) and chrysazin (**4**), and describes their spectroscopic and electrochemical properties. Experimental data are supported with DFT and TD-DFT calculations of molecular geometry, electronic structure and excited state properties. All DHAQs, due to the presence of an electron donor (phenolic) and electron acceptor (quinone) moieties, can be considered as electrochemically amphoteric species. This type of molecules is especially interesting from the point of view of molecular electronics [54].

## 2. Experimental

### 2.1. Materials and methods

All the organic dyes were of the highest purity available and used as purchased. Dye **1** was delivered by *Acros Organics* whereas **2**, **3** and **4** were supplied by *Alfa Aesar*. HPLC grade solvents of 99.9% purity were purchased from *POCH* (acetonitrile, ACN) and *Sigma–Aldrich* (dimethylformamide, DMF). The absorption spectra of dyes dissolved in either ACN or DMF were recorded on Agilent 8453 (*Agilent*, USA) spectrophotometer in quartz cell of 1 cm optical path length. Luminescence spectra were recorded on Fluoromax-4P (*Horiba Jobin Yvon*, France) spectrofluorimeter, in quartz cell of 1 cm optical path length. Diffuse reflectance spectra were recorded on Lambda 950 spectrophotometer (*Perkin Elmer*, USA) equipped with 150 mm integration sphere. For reflectance spectroscopy the samples were dispersed in spectrally pure $BaSO_4$. To obtain homogenous sample the dyes in a first step were dissolved in ACN or DMF before grinding with $BaSO_4$. The same $BaSO_4$ was used as a white standard. Recorded reflectance values were converted to the Kubelka–Munk function ($\alpha'_{KM}$) according to Eq. (1):

$$\alpha'_{KM}(h\nu) = \frac{[1 - R(h\nu)]^2}{2R(h\nu)}, \quad (1)$$

where $R$ stands for reflectance. The resulting spectra were multiplied by the energy of light quanta ($h\nu$) in order to preserve the Gaussian envelope of electronic transitions [55]:

$$\alpha_{KM}(h\nu) = \alpha'_{KM}(h\nu)\cdot h\nu. \quad (2)$$

Infrared spectra were obtained by Equinox 55 FTIR spectrophotometer (*Bruker*, USA) in KBr pellets. Electrochemical measurements were carried out with Autolab PGSTAT302N (*Metrohm Autolab*, The Netherlands) potentiostat. Differential pulse voltammetry (DPV) was conducted in a three electrode configuration. A platinum disc (1 mm diameter), a Pt wire and an Ag/AgCl electrode were used as working, counter and reference electrodes, respectively. All experiments were performed in DMF solution using 0.1 M tetrabutylammonium tetrafluoroborate ($TBABF_4$) as a supporting electrolyte, whereas the studied compounds were at *ca.* 1 mM concentration. Ferrocene was used as an internal reference. All potentials are given *vs.* standard hydrogen electrode (SHE) using the standard potential of ferrocene equal to 0.951 V [56]. Before the experiment the electrolyte was purged with nitrogen for at least half an hour and during measurement a nitrogen blanket was used to prevent contamination of the sample.

### 2.2. Computational details

The geometry optimization in the ground state was performed by the density functional theory (DFT) using the B3PW91 hybrid functional (Becke three parameter Perdew-Wang 1991) and the 6-311+G(d,p) basis set [57,58] with linear response method implementing integral equation formalism polarizable continuum model (LR-IEFPCM) [59]. Initial calculations were carried out with 3 different functionals (B3LYP, PBE0 and B3PW91). The B3PW91 was chosen for geometry optimization and excited state determinations because this functional was able to reproduce the experimental results more exactly. For low-lying excited state determination and UV–Vis spectra evaluation the time dependent density functional theory (TD-DFT) was used. The vertical excitation energy was calculated for first 20 singlet states. The solvent effect was included in TD-DFT via the polarizable continuum model (LR-IEFPCM). Calculation have been performed with the Gaussian03 program package [60]. The IR spectra were calculated using the same functional (B3PW91) but a reduced base (3-21G). The IR calculations were carried out for first 50 states.

## 3. Results and discussion

The alizarin dyes are based on three six-membered carbon rings, the central quinone ring and two peripheral ones with two hydroxyls in various positions. All these molecules are coplanar and of similar bond lengths. In **1** and **4** the two carbonyl groups are significantly asymmetric: 124 *vs.* 122 pm and 126 *vs.* 122 pm in positions 9 and 10 for **1** and **4** respectively, while other derivatives show much higher symmetry when the carbonyl C=O bond length is considered. C–O bonds in hydroxyl groups are of almost the same length in all studied molecules, in **1** are slightly longer than the average. The O–H bonds in hydroxyl groups are of comparable length of *ca.* 99 pm, the only exception is **1** in which the OH in 2-postion is significantly shorter, *ca.* 97 pm than the other hydroxyls (Table 1).

The presence of two different redox-active moieties within one molecule implies the intramolecular charge transfer properties. The quinone moiety in DHAQs serves as an electron acceptor, while the phenolic groups are electron donors. This is substantiated by a significant asymmetry in charge distribution within studied molecules. These moieties are arranged in different configurations within molecules which is in turn responsible for specific properties of DHAQs dyes and may be especially important for their respective photoelectrochemical behavior at the surface of wide band gap semiconductors, *e.g.* $TiO_2$.

**Table 1**
Bonds lengths between the atoms of carbonyl and hydroxyl groups for **1**–**4** compounds.

| Name | Ground state | | |
|---|---|---|---|
| | $d_{C=O}$[a]/pm | $d_{C-O}$[b]/pm | $d_{O-H}$[c]/pm |
| **1** | (9)[d] 124.065 | (1) 133.857 | (1) 99.440 |
| | (10) 122.465 | (2) 134.591 | (2) 96.803 |
| **2** | (9) 124.360 | (1) 133.472 | (1) 99.452 |
| | (10) 124.085 | (4) 133.472 | (4) 99.452 |
| **3** | (9) 124.067 | (1) 133.406 | (1) 99.253 |
| | (10) 124.067 | (5) 133.406 | (5) 99.253 |
| **4** | (9) 125.802 | (1) 133.590 | (1) 98.739 |
| | (10) 122.184 | (8) 133.590 | (8) 98. 739 |

[a] Length of carbon to oxygen double bond in the carbonyl moiety.
[b] Length of carbon to oxygen single bond near the hydroxyl moiety.
[c] Length of oxygen to hydrogen bond in hydroxyl moiety.
[d] Values in parenthesis indicate position number in the DHAQ skeleton.

The asymmetry in charge distribution within the studied dyes can be easily elucidated from Mulliken population analysis and electric potential maps (Fig. S1–S4, Fig. 1). It can be noticed that the quinone moiety serves as a local intramolecular electron acceptor, while the terminal ring systems are electron donors. This results in the formation of a significant dipole moment. The Mulliken charges localized at carbonyl oxygen atom of **1** are −0.307 and −0.283, respectively (Fig. S1). The negative charge is in turn shifted towards the central ring as well as towards carbon atoms bonded with the hydroxyl group. Reduction of neutral anthraquinone molecule occurs mainly at the central ring, (Fig. 7). Considering the charge distribution among the quinone moiety of **1**, **2** and **4** a strong asymmetry is observed (Figs. S1, S2 and S4). In addition **1** shows diverse charge values at two oxygen atoms belonging to the hydroxyl groups, −0.384 and −0.265 in the first and second position, respectively. The charge distribution is responsible for the specific acid-base character of **1**, privileging the deprotonation in the second in comparison to the first position. The oxygen atom in position 9 endowed with a more negative charge is repelled from the central ring whereas the more positively charged oxygen in position 10 is closer to the molecule backbone. The opposite situation is observed for the oxygen atoms of the hydroxyl groups where the most negative atom in the first position is closer to the quinone moiety, and the less negatively charged atom in the second position is slightly more distant.

Compound **2** belongs to the $C_{2v}$ symmetry group (a double axis and a plane of symmetry are parallel to each other). There is a large dipole moment (2.72 D) along the main axis. The electrostatic potential distribution reveals two pairs of surface dipoles symmetrical with respect to the long axis, created by negatively charged area of oxygen atoms of the carbonyl as well as the hydroxyl groups and the positively charged area near the hydrogen atom from peripheral aromatic rings (Fig. 1). Charge distribution of substituted carbonyl and hydroxyl groups is identical at both sides of the long axis. It is straightforward that bond lengths among the same substituents are also identical, Table 1.

Compound **3** belongs to the $C_{2h}$ symmetry group (a double axis and a plane of symmetry are perpendicular to each other), which compared to $C_{2v}$ has an additional inversion subgroup. The surface electrostatic potential map has two pairs of surface dipoles, symmetrical relative to the center, (Fig. 1) thought the net dipole moment is zero. Due to the symmetry of substituent arrangement the charge gathered at both carbonyl moieties is identical and amounts −0.312 (Fig. S3). Mulliken charge located at both hydroxyl

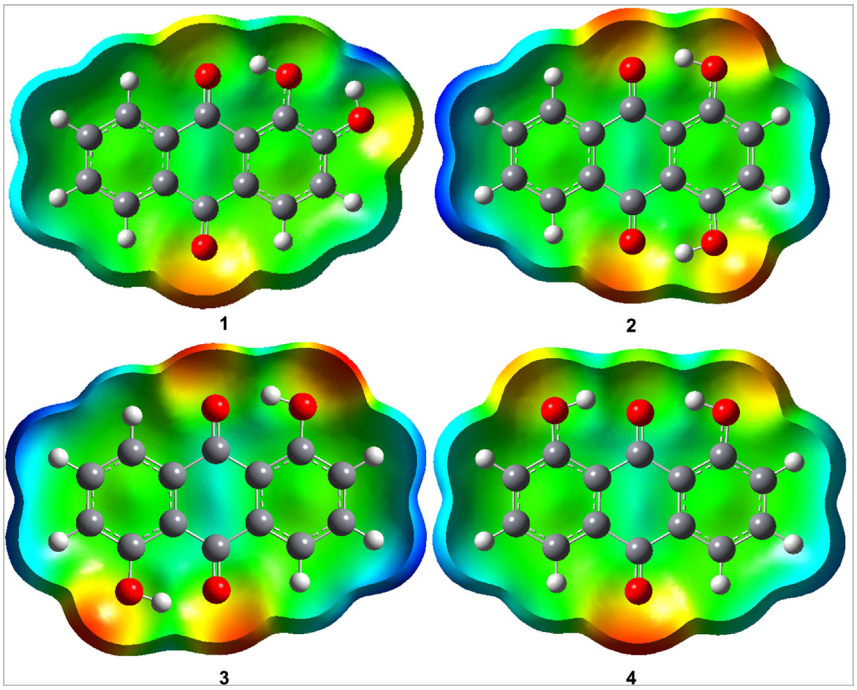


**Fig. 1.** Electrostatic potential mapped onto total electron density for the ground state of the studied DHAQs using DFT technique at the B3PW91/6-311 + G(d,p) level of theory. Areas marked in red and yellow gain electric charge, while cyan and blue are depleted of electron density in the ground state. Green color depicts neutral regions. Mulliken charges of individual atoms are available in the supplementary information (Figs. S1–S4). (For interpretation of the references to color in this figure legend, the reader is referred to the web version of this article.)

oxygen atoms also has the same value, −0.319. The C=O distance, equal for both carbonyl moieties, is identical to that of compound **2** (*cf.* Table 1).

Compound **4** belongs to the $C_{2v}$ symmetry group. The geometrical difference discloses in the direction of the symmetry axis, which is perpendicular to the molecule resulting in a negligible dipole moment with the value of 0.69 D along the symmetry axis. Charge distribution is uniform in the case of two hydroxyl groups (−0.331), whereas in the case of carbonyl atoms some differences can be observed (−0.389 and −0.264 of the 9-th and 10-th position, respectively). The carbonyl bond in the 9-th position is longer than in the 10-th position, the same can be observed as in the case of compound **1**.

The electron-donating properties of phenolic moieties within the dihydroxyanthraquinone series are embodied in the character of frontier orbitals. In all studied cases HOMOs are localized on the phenolic rings only (one ring in **1** and **2**, both terminal rings in **3** and **4**). It proves that HOMOs are strongly influenced by the position of hydroxyl groups. On the other hand LUMOs for all studied molecules are mainly localized on the central ring. Surprisingly, the contour of LUMOs does not depend on the position of hydroxyl substituents (Fig. 2). This result reflects the minor contribution of hydroxyl groups to the perturbation of aromatic bond framework, but it also indicates their dominant contribution to the electron-donating properties of studied compounds. Shapes of the HOMO and LUMO orbitals are similar in pairs: **1** and **2** on the one side (in which intramolecular transition is more significant) and **3** and **4** on the other.

### 3.1. Optical spectra of anthraquinone derivatives

UV–Vis absorption spectra of **1** and other DHAQs are relatively complex. The solution spectra usually show 1 electronic transition which can be assigned to a local excitation (LE) or an intramolecular charge transfer (ICT) transition. Furthermore, complex vibronic structure is usually observed upon deconvolution into Gaussian components. Aprotic solvents like ACN or DMF favor the neutral form of the dyes, however, minor contribution of deprotonated species or less stable tautomers is still possible. Similar phenomena were already observed in the case of carminic acid [53]. While deprotonated forms may be neglected, the different tautomers may additionally contribute to the complex shape of the absorption band envelope [36,51,52,61,62]. On the basis of literature reports and calculations presented in this paper (*cf.* electronic supplementary information), the presence of tautomeric forms is observed as new band at energy lower than the main transition. The bands assigned to the tautomers or other less stable forms are marked as light gray lines (Figs. 3–6). Solid spectra (recorded as diffuse reflectance and converted to Kubelka–Munk function) are usually less complex and reveal one dominant absorption maximum, much broader than in the case of spectra measured in liquid solutions. The broadening is a result of intermolecular interactions within the solid sample, which hinders the vibronic structure of absorption bands. The occurrence of an additional broad and low-intensity peak in the low energy part of spectra of **2** and **3** is interesting. This transition is present only in the solid state and can be ascribed to an intermolecular charge transfer band. This phenomenon is not observed in the solution because of greater distances between single molecules. This statement is supported by significant color changes during dissolution of **2** and **3** in ACN or DMF, respectively. Absorption spectra of studied dyes are shown in Figs. 3–6 and their main parameters are collected in Table 2.

Transition energies extracted from the liquid-phase spectrum of **1** show a very good agreement with the TD-DFT calculations. Both spectra reveal similar positions of significant electronic transitions which are compared in Fig. 3. Liquid solution spectrum presents three main transitions whereas in the solid state the number of transitions is the same but the one transition (3.21 eV) has low intensity. The TD-DFT computation allows the assignment of three

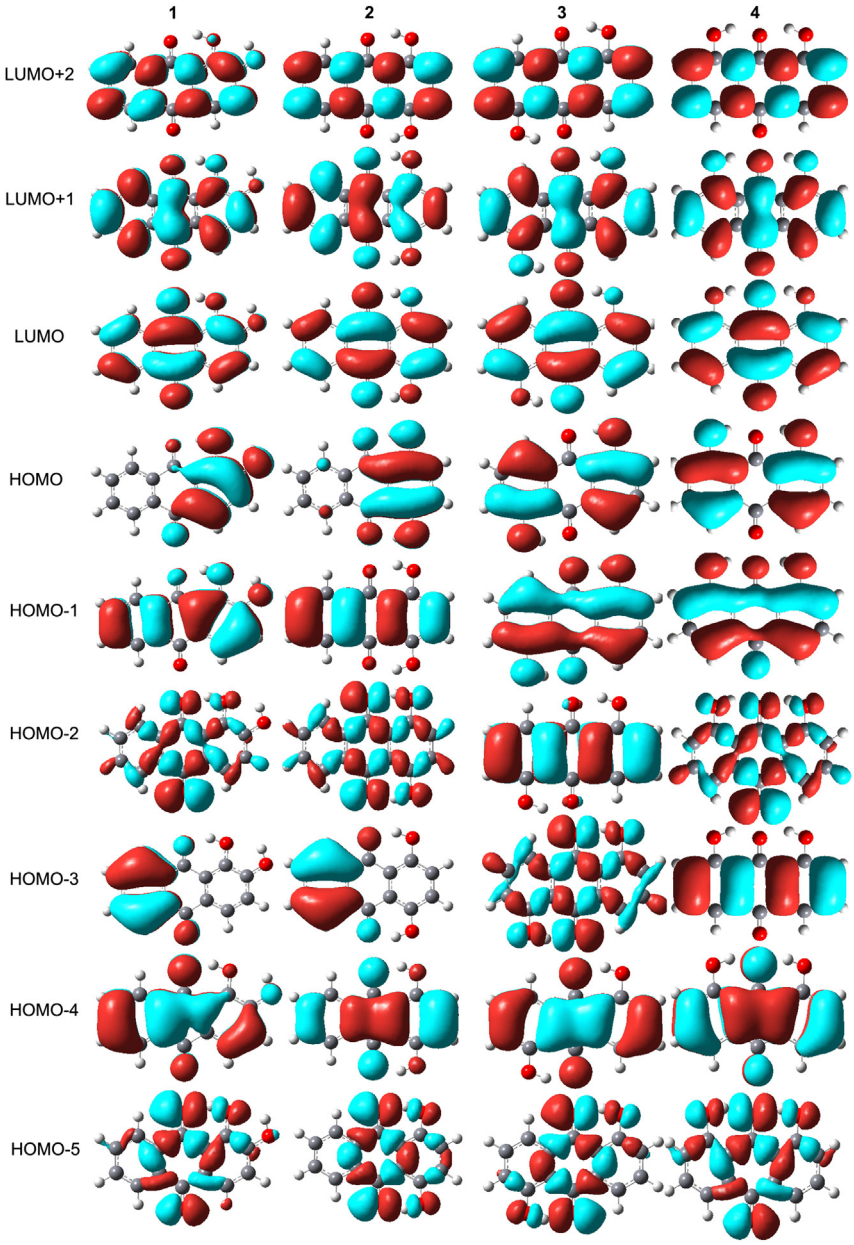


**Fig. 2.** Contours of the frontier molecular orbitals for studied dihydroxyanthraquinones calculated using DFT technique at the B3PW91/6-311 + G(d,p) level of theory.

components of the liquid spectra as the HOMO → LUMO, HOMO − 1 → LUMO, and HOMO − 3 → LUMO transitions. In the solid HOMO − 1 → LUMO has significantly lower amplitude (Fig. 3b). As a consequence of the overlapping of the considered orbitals the HOMO → LUMO and the HOMO − 3 → LUMO transitions have intramolecular charge transfer (ICT) character, while the HOMO − 1 → LUMO transition is of dominating local excitation (LE) character (*cf.* Fig. 2). The low-intensity peak at energy below the main HOMO → LUMO transition, shown as light gray line, belongs to one of the less stable tautomeric form (Fig. S5). Solid phase spectrum of **1** shows a significant bathochromic shift of all three principal transitions due to intermolecular interactions: π-stacking and/or hydrogen bonding. Lower energy transition is shifted by 0.06 eV, and the other two higher energy transition by 0.24 eV (Table 2). These interactions have the *J*-aggregate character. In the case of **1** a symmetric dimer with two hydrogen bonds can be formed. Such in-plane interaction is consistent with postulated *J*-type interaction between neighboring chromophores as reported by Yatsenko et al. [63]. Charge transfer between quinone moiety of one molecule with catechol functionality of the other by the intermolecular interaction should result in a bathochromic shift of the main absorption bands. Contribution from intermolecular charge transfer transition in the solid phase cannot be excluded.

In the case of **2** only one principal electronic transition can be extracted from combined experimental and theoretical data (Fig. 4). In liquid, the strong low energy transition at 2.56 eV can be assigned to HOMO → LUMO ICT transition. Moreover, in ACN a nicely resolved vibronic progression is observed. This is manifested as a series of equidistant Gaussian peaks with almost the same band width and gradually decreasing intensity. The spacing between peaks amounts to 1255 $cm^{-1}$. This energy value fits well with the highest peak in the fingerprint region (1257 $cm^{-1}$) responsible for the C–C–H and C–O–H bending vibrations, mainly within outer rings (Fig. S9). The solid phase spectrum presents one

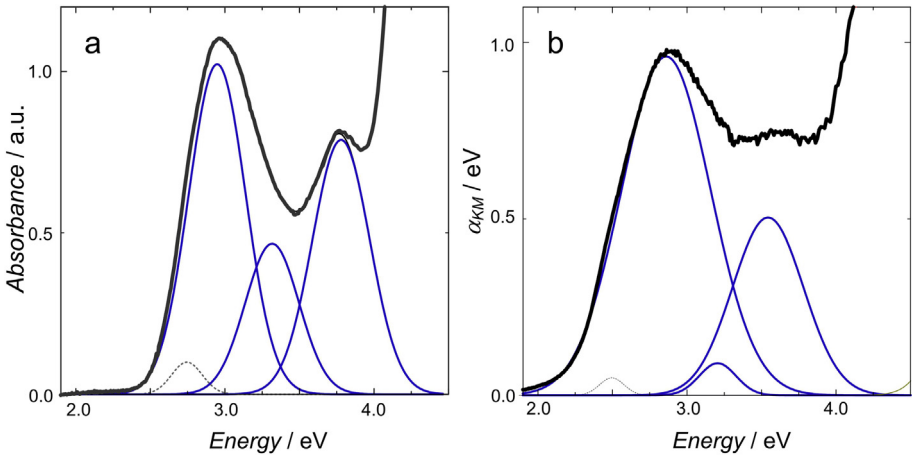


**Fig. 3.** UV–Vis spectra for 1 recorded in liquid ACN solution (a) and in the solid phase (b). Original experimental spectra are shown as heave black lines, while Gaussian components as blue lines. Contribution of tautomers is shown as light gray lines. (For interpretation of the references to color in this figure legend, the reader is referred to the web version of this article.)

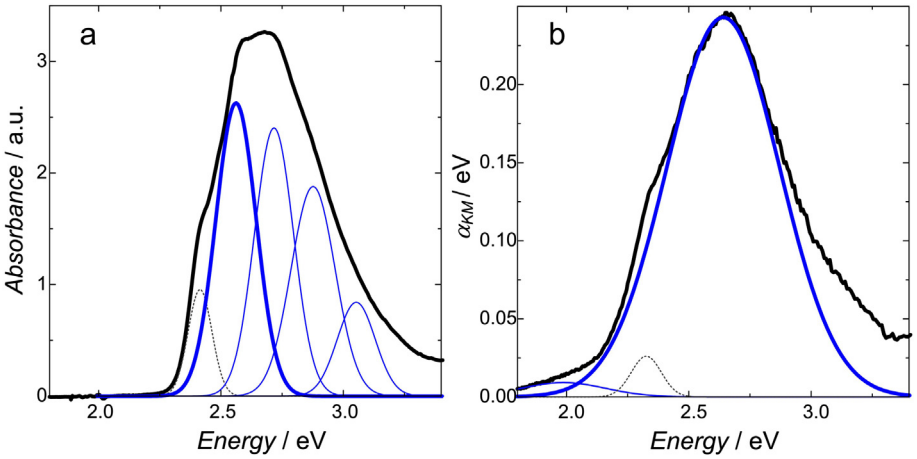


**Fig. 4.** UV–Vis spectra for **2** recorded in liquid ACN solution (a) and in the solid phase (b).

dominating peak. Solid state samples show complete lack of vibronic components, but the band is significantly broader. This broadening is associated with strong intermolecular interactions in solid. **2** presents an additional peak at an energy slightly lower than HOMO–LUMO. This transition can be ascribed to tautomeric structure (Fig. S6). The main transition peak for the solid sample shows hipsochromic shift of *ca.* 0.08 eV *vs.* liquid solution (Table 2). This shift can be again attributed to intermolecular interactions, but

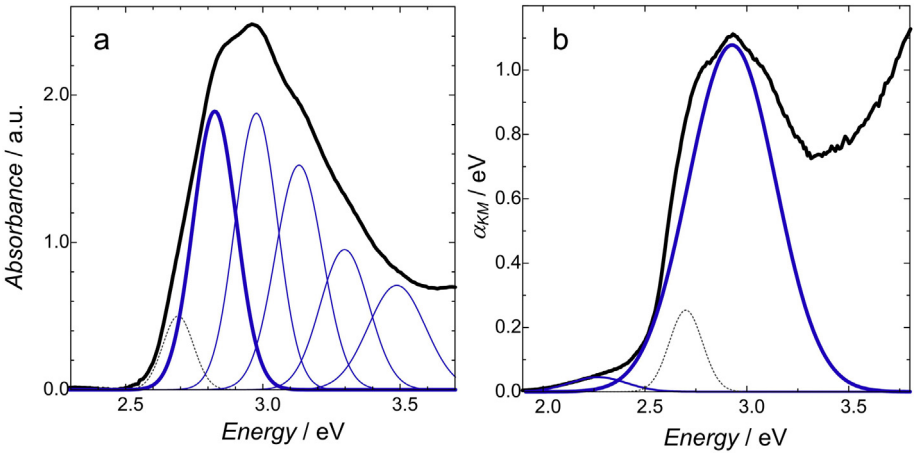


**Fig. 5.** UV–Vis spectra for **3** recorded in liquid DMF solution (a) and in the solid phase (b).

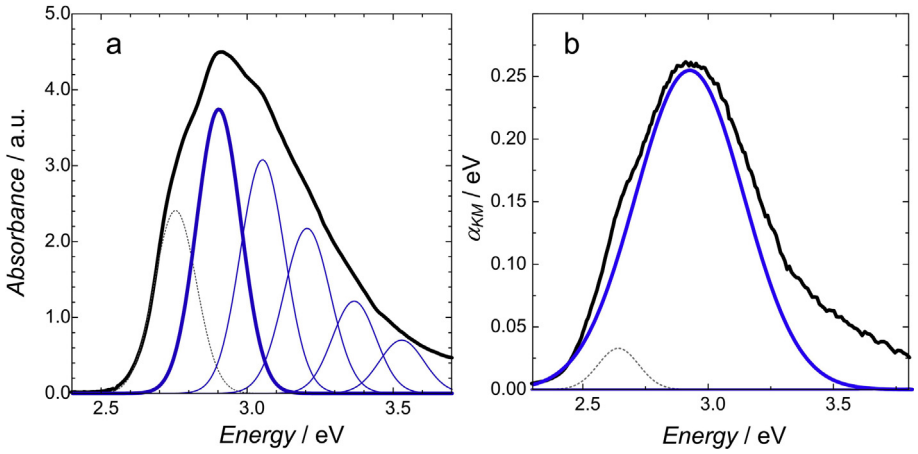


**Fig. 6.** UV–Vis spectra for **4** recorded in liquid ACN solution (a) and in the solid phase (b).

in this case of *H*-type aggregate character [63]. Furthermore, a broad absorption at *ca.* 1.9 eV is observed only for the solid sample, and may be attributed to charge transfer between individual molecules in the solid phase.

Similarly to quinizarin, the main electronic transitions of anthrarufin in DMF show a vibronic structure (Fig. 5). The most intense peak at 2.82 eV is associated with the HOMO → LUMO ICT transition. An additional transition at 2.69 eV appears both in liquid and solid phases. This transition is assigned to the tautomeric form of the dye (Fig. S7). The distance between peaks is about 1256 $cm^{-1}$. This vibronic progression can be associated with antisymmetrical C–O–H bending vibration of the outer rings at 1240 $cm^{-1}$ (Fig. S10). In the solid state the HOMO–LUMO transition is hipsochromically shifted to 2.93 eV as compared with the liquid state, and may be assigned to a significant contribution of *H*-type aggregates in the optical properties of solid **3**, in agreement with the results reported for **2**. Vibronic broadening is again visible at high energies. As found in **2** solid state spectra, a broad absorption is observed at lower energy region *ca.* 2.69 eV. This transition may be attributed to charge transfer between individual molecules in the solid phase.

The liquid-phase absorption spectrum of **4** is composed of six Gaussian components. The first peak at 2.75 eV is probably related to one of the tautomeric forms (Fig. S8). The 2.90 eV transition is the HOMO → LUMO transition vibronically splitted into five subsequent peaks. The vibronic components are separated by 1209 and 1230 $cm^{-1}$. Those frequencies are ascribed, to two antisymmetrical C–O–H bending vibrations at energies 1205 and 1270, respectively (Fig. S11). Both in the liquid and solid phase maxima remain almost at the same position (only 0.02 eV batochromic shift in solid spectra with respect to the liquid), what means that aggregation is barely observed.

Theoretically obtained energy values fit the experimental results remarkably well in all cases. For **1** and **2**, the differences being 0.09 and 0.08 eV respectively whereas for **3** and **4** only 0.04 and 0.05 eV (Table 2). Comparing spectral line shapes in the solution, **1** seems to have different, more regular character than the others (no visible vibronic bands).

Comparing absorption spectra of all the studied compounds, **2** has an absorption maximum visibly shifted towards lower energies. Besides, all the lowest energy electronic transitions have an ICT character. This can be deduced from the profiles of frontier orbitals, but can be clearly understood from the contours of the Fukui function. Fukui functions $f^{+}(r)$ and $f^{-}(r)$ have been calculated using the frozen orbital approximation as [64,65]:

$$f^{+}(r) = |\psi_{\mathrm{LUMO}}(r)|^2 \tag{3}$$

and

$$f^{-}(r) = \left|\psi_{\mathrm{HOMO}}(r)\right|^2 \tag{4}$$

This simple method, which assumes that frontier orbital contours are not sensitive to small changes in electric charge, allows

**Table 2**
Comparison of experimental and calculated (TD-DFT) electronic transitions for 1, 2, 3 and 4 (absorption of tautomers and transitions with negligible oscillation strength are omitted).

| Molecule/Peak | Liquid solution (ACN) | | Solid phase | Calculations (ACN) | | | | |
|---|---|---|---|---|---|---|---|---|
| | $E_{h\nu}$[a] | $\nu_{osc}$ ($cm^{-1}$)[b] | $E_{h\nu}$[a] | TD-DFT[c] | $f$[d] | Transition[e] | Δ[f] | $\nu_{osc}$ ($cm^{-1}$)[g] |
| **1**/1 | 2.92 | – | 2.86 | 2.83 | 0.1409 | H → L | 0.09 | – |
| **1**/2 | 3.27 | – | 3.21 | 3.37 | 0.0395 | H(−1) → L | 0.10 | – |
| **1**/3 | 3.78 | – | 3.54 | 3.76 | 0.0788 | H(−3) → L | 0.02 | – |
| **2**/1 | 2.56 | 1255 | 2.64 | 2.64 | 0.2226 | H → L | −0.08 | 1257 |
| **3**/1 | 2.82 | 1256 | 2.93 | 2.86 | 0.2973 | H → L | −0.04 | 1240 |
| **4**/1 | 2.90 | 1209/1230 | 2.92 | 2.85 | 0.2794 | H → L | 0.05 | 1205/1270 |

[a] Experimental maximum of the transition energy (eV).
[b] Distance between peaks of oscillation structure (eV).
[c] Theoretical maximum of the transition energy (eV).
[d] Oscillator strength.
[e] Type of the transition H – HOMO, L – LUMO.
[f] Difference between experimental (liquid) and theoretical value (eV).
[g] Oscillation values obtained from calculated IR spectra.

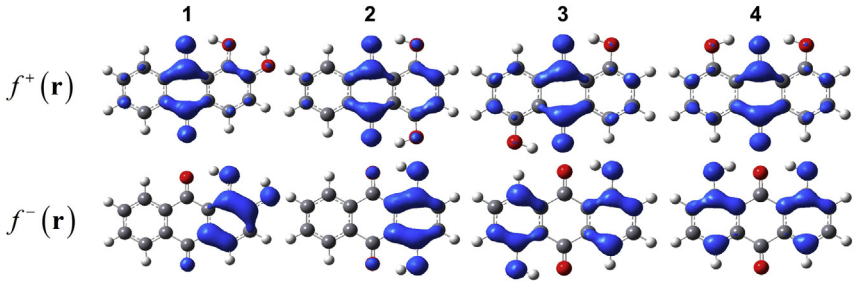


**Fig. 7.** Spatial distributions of Fukui functions $f^+(r)$ and $f^-(r)$ calculated for studied compounds at the B3PW91/6-311+G(d,p) level of theory.

computation of Fukui functions in one step. Hereby calculated Fukui functions are shown in Fig. 7.

It can be clearly seen that in all studied cases the $f^+(r)$ function is localized on the central ring (quinone moiety), while the $f^-(r)$ function on phenolic rings. Therefore it can be concluded that the central moiety acts as an electron acceptor, while aromatic rings with hydroxyl substituents act as electron donors.

All studied compounds are rather poor lumophores with average quantum yields of *ca.* $\Phi = 0.025$ except for **2** whose emission quantum yield is one order of magnitude higher ($\Phi = 0.120$) [22]. Low fluorescence quantum yields are the result of the specific energy level arrangement *i.e.*, of the relatively high $T_2$ state, which significantly contributes to intersystem crossing [22]. The luminescence spectra are further complicated by the presence of the tautomeric forms of the studied dyes and by the possible contribution of excited state intramolecular proton transfer (ESIPT) processes (Fig. 8).

The large reorganization energy leads to conclusion that the geometry of molecules in the ground and excited state differs considerably (Table 3). It can be noticed, however, that the molecules with intramolecular hydrogen bonds and high symmetry are characterized with lower reorganizational energies (**2** and **4**). In the case of **2** it is also manifested in smallest charge redistribution upon excitation (*vide infra*). While these data just roughly present the extent of reorganization of electronic charge (and following geometry adjustment) more detailed data are obtained by mapping the changes in the electrostatic potential upon excitation over the total electron density. These results are presented in Fig. 10 (*vide infra*).

On the first sight compounds **1** and **3** have very similar shape of fluorescence spectra, (Fig. 8a and c), with one clear emission maxima and poorly resolved vibronic structure. On the other hand **2** and **4** present quite different luminescence pattern with two distinct emission maxima. This behavior can be tentatively explained by ESIPT process as previously postulated by Demchenko

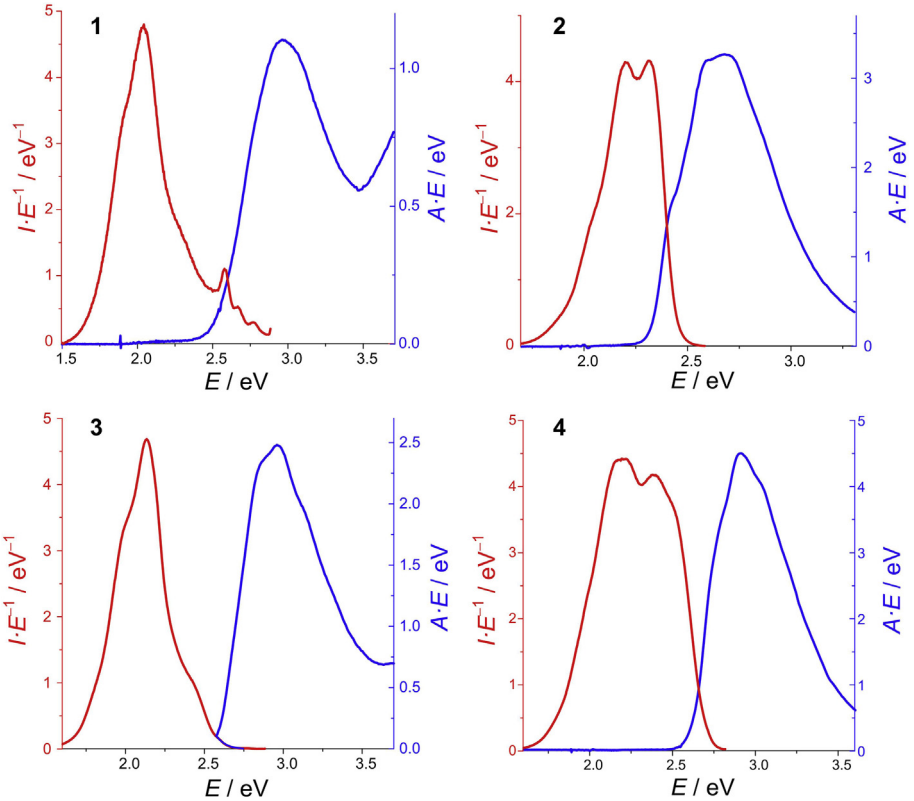


**Fig. 8.** Fluorescence *vs.* absorption spectra for DHAQs dissolved in ACN (except anthrarufin, which is dissolved in DMF). The excitation energy is 420 nm (2.95 eV), 470 nm (2.64 eV), 420 nm (2.95 eV) and 430 nm (2.88 eV) for **1**, **2**, **3** and **4**, respectively.

**Table 3**
Stokes shifts are evaluated as the difference between experimental absorption and fluorescence maxima.

| Name | Stokes shift | | Reorganization energy | |
|---|---|---|---|---|
| | eV | $cm^{-1}$ | eV | $cm^{-1}$ |
| **1** | 0.96 | 7710 | 0.48 | 3855 |
| **2** | 0.42 | 3373 | 0.21 | 1687 |
| **3** | 0.85 | 6809 | 0.43 | 3405 |
| **4** | 0.60 | 4811 | 0.30 | 2406 |

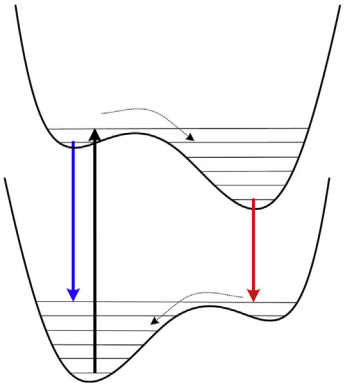

**Fig. 9.** Schematic representation of dual emission in the case of ESIPT process.

[66]. Upon excitation intramolecular proton transfer reaction accompanied with electron density reorganization may lead to a tautomeric form which is less stable in the ground state (Fig. 9). This form should be then characterized with excited state energy. As a result a new tautomeric equilibrium sets in and then emission from both species is concomitantly observed. In this case, however, the emission spectrum is independent of the excitation energy. It is therefore reasonable, that molecules which undergo dual emission are characterized by lower Stokes shift, as one of the emissive states retains mostly the ground state geometry, while the other is strongly reorganized. This is the case of **2** and **4**. On the other hand, large Stokes shifts do not exclude the ESIPT process, but rather indicate, that proton transfer is much more efficient and the state with initial geometry vanishes before any luminescence can be observed. Stokes shifts can be regarded as a measure of total reorganization energy (Table 3). It can be noticed that the highest value of Stokes shift (*i.e.*, the highest total reorganization energy) is observed in the case of **1**, while other dyes (especially **2**) show much lower Stokes shifts [67–69].

Redistribution of electron density upon excitation can be visualized as a change in electrostatic potential (Fig. 10). It can be clearly seen that changes in electrostatic potential are in partial agreement with frontier orbital character and spatial arrangement of Fukui functions. The lowest excitation results in an increment of the negative charges in the quinone moiety (central ring), while the areas with phenolic groups acquire positive charge. In the case of **1** the close proximity of the OH group to one of the carbonyls results in marked asymmetry in the charge distribution in the excited state – the 10-position carbonyl becomes strongly negative, while the 9-position becomes positive together with the catecholate system. Similar charge redistribution can be observed in the case of **4**. In **2** the distribution of electron density is virtually the same as in the ground state, which is also reflected in the lower value of reorganization energy. The intramolecular hydrogen bonding involving both carbonyls, may lead to strong configurational mixing between ground and excited state. Therefore only the external rings of the molecule are significantly changed upon excitation. **3** behaves exactly as expected from a simple analysis: both phenolic moieties act as electron donors, while the quinonic ring is the sole electron acceptor. Interactions of hydroxyl groups with carbonyl oxygen atoms decrease the electron acceptor properties of the quinone moiety in **2** and only slight redistribution of electrostatic potential upon excitation is observed.

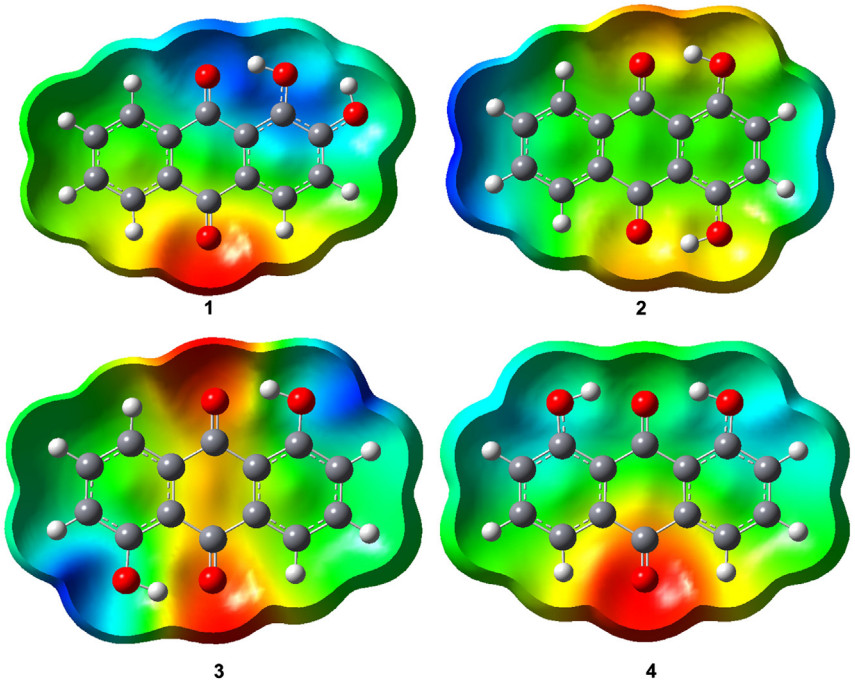


**Fig. 10.** Differential electrostatic potential mapped onto the electron density isosurfaces. Areas marked in red and yellow gain electric charge, while cyan and blue are depleted of electron density upon excitation. (For interpretation of the references to color in this figure legend, the reader is referred to the web version of this article.)

### 3.2. Electrochemistry

Differential pulse voltammetry (DPV) reveals better sensitivity and discriminates non-faradic current and therefore is preferable to determine oxidizing potentials instead of more common cyclic voltammetry. It is also a preferred technique in the case of poor reversibility of electrode processes, *e.g.* due to rapid secondary processes, as usually observed in the case of organic radicals. Quinone and hydroxyl species of DHAQs participate in the reduction and oxidation processes respectively. At negative potentials usually we observe two peaks which can be associated with two consecutive one-electron reductions (Fig. 11). The first reduction peak is ascribed to the one-electron process of anion radical form obtained as follows:

$$AQ + e^- \rightarrow AQ^{\bullet -} \quad (5)$$

The second peak at more negative potentials reflects second reduction step leading to formation of dianions:

$$AQ^{\bullet -} + e^- \rightarrow AQ^{2-} \quad (6)$$

Aprotic solvent should prevent protonation processes even at low potentials. **1** is the hardest reduced compound. The first reduction peak of **1** occurs at potential −0.04 V, much lower than other compounds with reduction values ranging from 0.1 ÷ 0.18 V. The second reduction peak is of lower intensity than the first one probably due to the scarce stability of anion radicals and/to quinhydrone-like dimer formation [70]

$$2AQ^{\bullet -} = \{AQAQ\}^{2-} \quad (7)$$

Applied positive potential leads to oxidation of hydroxyl groups. In all studied cases two subsequent one-electron steps are observed, usually the second peak has much lower intensity than the first one, also due to instability and reactivity of intermediate species. First oxidation potentials of all studied compounds are almost identical (*ca.* 1.4 V) and comparable with pure anthraquinone. DHAQs are good electron acceptors because of low-lying LUMOs.

According to the Latimer-type diagrams the reduction potentials in the excited state are: 2.47, 2.53, 2.76, 2.75 V for **1**, **2**, **3**, and **4** respectively, Fig. 12. Oxidation potentials in excited state are: −1.10, −0.96, −1.14, and −1.28 V for **1**, **2**, **3** and **4**. It can be clearly read out that in **3** and **4** excited state are the best donors and acceptors at the same time.

## 4. Conclusions

Alizarin and its isomers reveal a lot of common features as a consequence of the same structural core: the anthraquinone moiety. All the studied compound show strong HOMO–LUMO ICT transitions, which are also weakly emissive. However, in some aspects they surprisingly differ. Specific arrangement of hydroxyl substituents can switch ON or OFF the dual emission phenomenon being a result of interplay between excited state deactivation and rearrangement. Charge distribution in the ground state reveals significant dipole moment, able to stimulate weak interactions *e.g.* physisorption, in **1** and **2**, and dipole moment close to zero in **3** and **4**. Evolution of charge distribution upon excitation strongly depends on intramolecular interactions. Frontier orbitals involved in the lowest energy transitions indicate CT character for all examined compounds. Geometry affects also the electron affinity of studied species, with **2** and **3** being easily reducible while **1** is the hardest to reduce.

Versatility of molecular properties in a family of closely related compounds renders them good candidates for further studies as modifiers for various oxide-based semiconductors. The anthraquinone family offers a wide range of excited state properties that can modulate the photoelectrochemistry of a hybrid system with preserved (in most cases) photosensitizer-semiconductor binding mode.

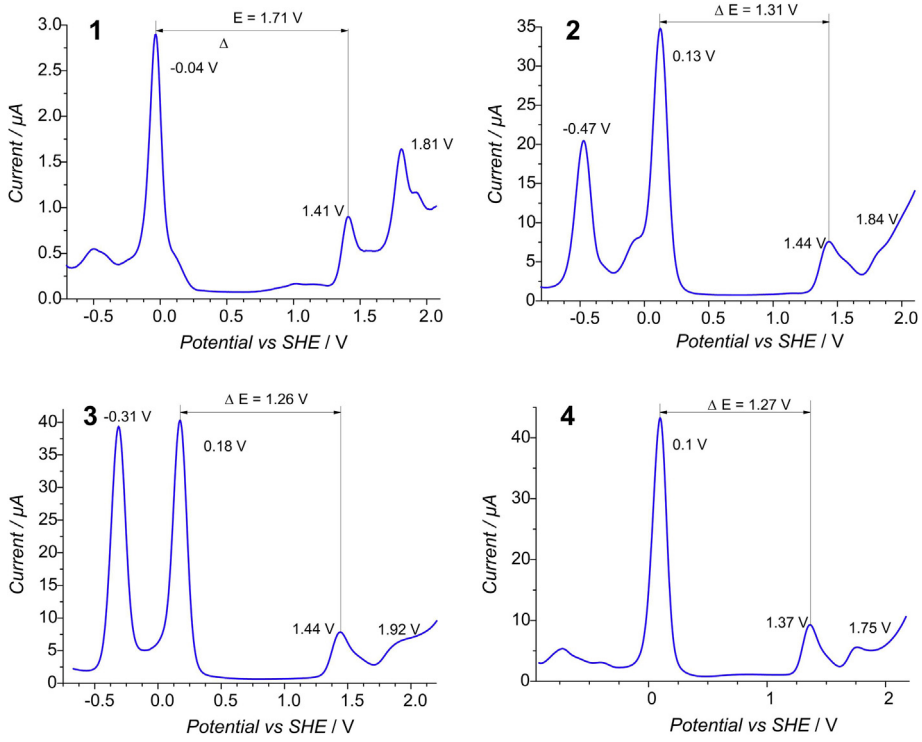


**Fig. 11.** DPV voltammograms of dihydroxyanthraquinones.

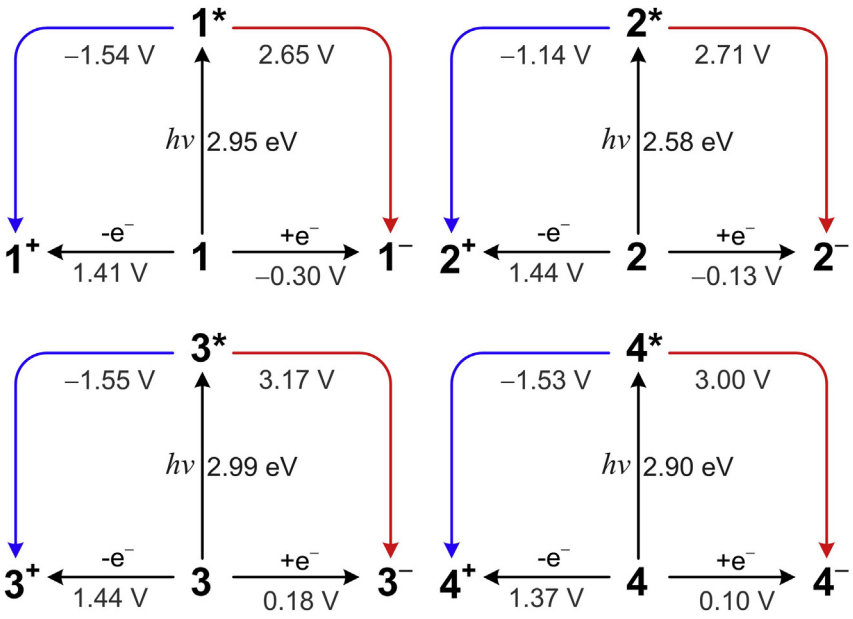


**Fig. 12.** Latimer-type diagrams of oxidation and reduction potentials in the ground and excited state for studied dyes. The *hν* energy was taken from intercept of the absorbance and fluorescence spectra.

## Acknowledgments

Authors thank Prof. Dr. Ewa Brocławik and Dr. Ewa Wasielewska for valuable comments and discussion. Financial support from National Science Centre (grants ℳ DEC-2011/03/B/ST5/01495 and 2011/03/N/ST5/04470) and AGH University of Science and Technology (contract ℳ 11.11.180.509) is gratefully acknowledged. J.M. thanks Malopolska Scholarship Fund for PhD students (ℳ ZS.4112-212/2010). The computational part of this paper was supported in parts by PL-Grid Infrastructure and by Academic Computer Centre CYFRONET AGH within computational grant MEiN/SGI3700/UJ/085/2006.

## Appendix A. Supplementary data

Supplementary data related to this article can be found at http://dx.doi.org/10.1016/j.dyepig.2013.12.009.

## References

[1] Serpone N, Emeline AV. Semiconductor photocatalysis – past, present, and future outlook. J Phys Chem Lett 2012;3:673–7.
[2] Kamat PV, Tvrdy K, Baker DR, Radich JG. Beyond photovoltaics: semiconductor nanoarchitectures for liquid-junction solar cells. Chem Rev 2010;110:6664–88.
[3] Szaciłowski K. Infochemistry: information processing at the nanoscale. John Wiley & Sons, Ltd; 2012.
[4] Eberle AR, Lerner MW. Separation and determination of scandium spectrophotometric method using Alizarin red S. Anal Chem 1955;27(10):1551–4.
[5] Crossley ML. Certain metallic derivatives of hydroxy-anthraquinones. J Am Chem Soc 1919;41:2083–90.
[6] Kubo Y, Ishida T, Kobayashi A, James TD. Fluorescent alizarin–phenylboronic acid ensembles: design of self-organized molecular sensors for metal ions and anions. J Mater Chem 2005;15:2889–95.
[7] Natelson S, Penniall R. Colorimetric estimation of ultramicro quantities of calcium in human serum as the complex with alizarin. Anal Chem 1955;27:434–7.
[8] Rozin YA, Tat'yanenko LV, Buryndina EI, Barybin AS, Popova VG. Alizarin derivatives as inhibitors of calcium transport. Pharm Chem J 1996;30:520–2.
[9] Gregory CA, Gunn WG, Peister A, Prockop DJ. An Alizarin red-based assay of mineralization by adherent cells in culture: comparison with cetylpyridinium chloride extraction. Anal Biochem 2004;329:77–84.
[10] Green OR. A manual of practical laboratory and field techniques in palaeobiology. Springer; 2010.
[11] Wu L, Forsling W, Holmgren A. Surface complexation of calcium minerals in aqueous solution. 4. The complexation of Alizarin Red S at fluorite–water interfaces. J Colloid Interface Sci 2000;224:211–8.
[12] Palomares E, Vilar R, Green A, Durrant JR. Alizarin complexone on nanocrystalline $TiO_2$: a heterogenous approach to anion sensing. Adv Funct Mater 2004;14:111–6.
[13] Schafer HNS. Application of ion exchange to analysis of phosphate rocks. Anal Chem 1963;35:53–6.
[14] Ashley RP. Zirconyl-alizarin chelate in spectrophotometric determination of trace amounts of fluorine. Anal Chem 1960;32:834–6.
[15] Xu ZC, An JY, Hu YZ, Tian F. Photoinduced one-electron reduction of 1,4-dihydroxyanthraquinone. Chin Chem Lett 2000;11:479–82.
[16] Quinti L, Allen NS, Edge M, Murphy BP, Perotti A. A study of the strongly fluorescent species formed by the interaction of the dye 1,4-dihydroxyanthra quinone (quinizarin) with Al(III). J Photochem Photobiol A 2003;155:79–91.
[17] Idriss KA, Hashem EY, Abdel-Azizb MS, Ahmed HM. Direct spectrophotometric determination of aluminium oxide in Portland cement and cement clinker. An insight into the solution equilibria and analytical aspects of the aluminium–quinizarin system. Analyst 2000;125:221–5.
[18] Ladell P. Isolation and characterization of antibiotics produced by the nematode symbiont Xenorhabdus szentrimaii. Master of Science in Biology thesis. University of Wisconsin-La Crosse; 2011.
[19] Say-Liang-Fat S, Cornard J-P, Moncomble A. Study on chrysazin–aluminium(III) interaction in solution by spectroscopy and quantum chemical calculations. Polyhedron 2012;48:237–44.
[20] Liu G, Li X, Zhao J, Horikoshi S, Hidaka H. Photooxidation mechanism of dye alizarin red in $TiO_2$ dispersions under visible illumination: an experimental and theoretical examination. J Mol Catal 2000;153:221–9.
[21] Batchelor-McAuley C, Dimov IB, Aldous L, Compton RG. The electrochemistry of quinizarin revealed through its mediated reduction of oxygen. Proc Natl Acad Sci U S A 2011;108:19891–5.
[22] Gollnick K, Held S, Mártire DO, Braslavsky SE. Hydroxyanthraquinones as sensitizers of singlet oxygen reactions: quantum yields of triplet formation and singlet oxygen generation in acetonitrile. J Photochem Photobiol A 1992;69:155–65.
[23] Perassolo M, Quevedo CV, Busto VD, Giulietti AM, Talou JR. Role of reactive oxygen species and proline cycle in anthraquinone accumulation in Rubia tinctorum cell suspension cultures subjected to methyl jasmonate elicitation. Plant Physiol Biochem 2011;49:758–63.
[24] Di Iorio Y, Brusa MA, Feldhoff A, Grela MA. Electron transfer from photoexcited $TiO_2$ to chelating alizarin molecules: reversible photochromic effect in Alizarin@$TiO_2$ under UV irradiation. Chem Phys Chem 2009;10:1077–83.
[25] Vaik K, Mäeorg U, Maschion FC, Maia G, Schiffrin DJ, Tammeveski K. Electrocatalytic oxygen reduction on glassy carbon grafted with anthraquinone by anodic oxidation of a carboxylate substituent. Electrochim Acta 2005;50:5126–31.
[26] Seinberg J-M, Kullapere M, Mäeorg U, Maschion FC, Maia G, Schiffrin DJ, et al. Spontaneous modification of glassy carbon surface with anthraquinone from the solutions of its diazonium derivative: an oxygen reduction study. J Electroanal Chem 2008;624:151–60.

[27] Di Iorio Y, Parra R, Szaciłowski K, Grela MA. Alizarin complexone: an interesting ligand for designing $TiO_2$ – hybrid nanostructures. New J Chem 2013;37:969–76.
[28] Di Iorio Y, Rodríguez HB, Román ES, Grela MA. Photoelectrochemical behavior of alizarin modified $TiO_2$ films. J Phys Chem C 2010;114:11515–21.
[29] Duncan WR, Prezhdo OV. Nonadiabatic molecular dynamics study of electron transfer from alizarin to the hydrated $Ti^{4+}$ ion. J Phys Chem B 2005;109:17998–8002.
[30] Duncan WR, Stier WM, Prezhdo OV. Ab initio nonadiabatic molecular dynamics of the ultrafast electron injection across the alizarin-$TiO_2$ interface. J Am Chem Soc 2004;127:7941–51.
[31] Sánchez-de-Armas R, Oviedo J, Miguel MÁS, Sanz JF. Direct vs indirect mechanisms for electron injection in dye-sensitized solar cells. J Phys Chem C 2011;115:11293–301.
[32] Sánchez-de-Armas R, San-Miguel MA, Oviedo J, Sanz JF. Direct vs. indirect mechanisms for electron injection in DSSC: catechol and alizarin. Comput Theor Chem 2011;975:99–105.
[33] Huber R, Moser J-E, Grätzel M, Wachtveitl J. Real-time observation of photoinduced adiabatic electron transfer in strongly coupled dye/semiconductor colloidal systems with a 6 fs time constant. J Phys Chem B 2002;106:6494–9.
[34] Duncan WR, Prezhdo OV. Theoretical studies of photoinduced electron transfer in dye-sensitized $TiO_2$. Annu Rev Phys Chem 2007;58:143–84.
[35] Kaniyankandy S, Verma S, Mondal JA, Palit DK, Ghosh HN. Evidence of multiple electron injection and slow back electron transfer in alizarin-sensitized ultrasmall $TiO_2$ particles. J Phys Chem C 2009;113:3593–9.
[36] Preat J, Laurent AD, Michaux C, Perpète EA, Jacquemin D. Impact of tautomers on the absorption spectra of neutral and anionic alizarin and quinizarin dyes. J Mol Struct 2009;901:24–30.
[37] Sánchez-de-Armas R, López JO, San-Miguel MA, Sanz JF. Real-time TD-DFT simulations in dye sensitized solar cells: the electronic absorption spectrum of alizarin supported on $TiO_2$ nanoclusters. J Chem Theory Comput 2010;6:2856–65.
[38] Li J, Kondov I, Wang H, Thoss M. Theoretical study of photoinduced electron-transfer processes in the dye-semiconductor system alizarin-$TiO_2$. J Phys Chem C 2010;114:18481–93.
[39] Szaciłowski K, Macyk W. Chemical switches and logic gates based on surface modified semiconductors. C R Chim 2006;9:315–24.
[40] Szaciłowski K, Macyk W. Photoelectrochemical photocurrent switching effect: a new platform for molecular logic devices. Chimia 2007;61:831–4.
[41] Gawęda S, Kowalik R, Kwolek P, Macyk W, Mech J, Oszajca M, et al. Nanoscale digital devices based on the photoelectrochemical photocurrent switching effect: preparation, properties and applications. Isr J Chem 2011;51:36–55.
[42] Gawęda S, Podborska A, Macyk W, Szaciłowski K. Nanoscale optoelectronic switches and logic devices. Nanoscale 2009;1:299–316.
[43] Macyk W, Stochel G, Szaciłowski K. Photosensitization and photocurrent switching effect in nanocrystalline titanium dioxide functionalized with iron(II) complexes: a comparative study. Chem Eur J 2007;13:5676–87.
[44] Mech J, Kowalik R, Podborska A, Kwolek P, Szaciłowski K. Arithmetic device based on multiple Schottky-like junctions. Aust J Chem 2010;63:1330–3.
[45] Oszajca M, Kwolek P, Mech J, Szaciłowski K. Substituted polyacenes as prospective modifiers of $TiO_2$ surface. Curr Phys Chem 2011;1:242–60.
[46] Oszajca M, McCall KL, Robertson N, Szaciłowski K. Photocurrent switching effects in $TiO_2$ modified with ruthenium polypyridine complexes. J Phys Chem C 2011;115:12187–95.
[47] Podborska A, Oszajca M, Gawęda S, Szaciłowski K. Nanoparticles with logic and numeracy: towards 'computer-on-a-particle' optoelectronic devices. IET Circuits Devices Syst 2011;5:103–14.
[48] Podborska A, Szaciłowski K. Towards 'computer-on-a-particle' devices: optoelectronic 1:2 demultiplexer based on nanostructured cadmium sulfide. Aust J Chem 2010;63:1330–3.
[49] Szaciłowski K. Digital information processing in molecular systems. Chem Rev 2008;108:3481–548.
[50] Szaciłowski K, Macyk W, Stochel G. Light-driven OR and XOR programmable chemical logic gates. J Am Chem Soc 2006;128:4550–1.
[51] Savko M, Kaščáková S, Gbur P, Miškovský P, Uličný J. Performance of time dependent density functional theory on excitations of medium sized molecules – test on ionic forms of anthraquinone dihydroxy derivatives. J Mol Struct 2007;823:78–86.
[52] Dabsu TK. Tautomersim and spectral properties of alizarin (1,2-dihydroxyanthracene-9, 10-dione). Master of Science in Chemistry thesis. Addis Ababa University; 2007.
[53] Gawęda S, Stochel G, Szaciłowski K. Photosensitization and photocurrent switching in carminic acid/titanium dioxide hybrid material. J Phys Chem C 2008;112:19131–41.
[54] Bendikov M, Wudl F, Perepichka DF. Tetrathiafulvalenes, oligoacenenes, and their buckminsterfullerene derivatives: the brick and mortar of organic electronics. Chem Rev 2004;104:4891–945.
[55] Endicott JF. Molecular electron transfer. In: McCleverty JA, Meyer TJ, editors. Comprehensive coordination chemistry II. Amsterdam: Elsevier; 2003. pp. 657–730.
[56] Tsierkezos NG. Cyclic voltammetric studies of ferrocene in nonaqueous solvents in the temperature range from 248.15 to 298.15 K. J Solut Chem 2007;36:289–302.
[57] Eloranfa J, Vatanen V, Gronroos A, Vuolle M, Makela R, Heikkila H. Comparison of spin density calculation methods for various alkyl-substituted 9,10-anthraquinone anion radicals in the solution phase. Magn Reson Chem 1996;34:898–902.
[58] Jacquemin D, Preat J, Charlot M, Wathelet V, André J-M, Perpète EA. Theoretical investigation of substituted anthraquinone dyes. J Chem Phys 2004;121:1736–43.
[59] Cancés E, Mennucci B, Tomasi J. A new integral equation formalism for the polarizable continuum model: theoretical background and applications to isotropic and anisotropic dielectrics. J Chem Phys 1997;107:3032–41.
[60] Frisch MJ, Trucks GW, Schlegel HB, Scuseria GE, Robb MA, Cheeseman JR, et al. Gaussian 03, Rev. D.01. Wallingford CT: Gaussian, Inc.; 2004.
[61] Douma DH, M'Passi-Mabiala B, Gebauer R. Optical properties of an organic dye from time-dependent density functional theory with explicit solvent: the case of alizarin. J Chem Phys 2012;137(15). 154314(1–5).
[62] Le Person A, Cornard J-P, Say-Liang-Fat S. Studies of the tautomeric forms of alizarin in the ground state by electronic spectroscopy combined with quantum chemical calculations. Chem Phys Lett 2011;517:41–5.
[63] Yatsenko AV, Chernyshev VV, Popov SI, Sonneveld EJ, Schenk H. Visible spectra of crystalline anthraquinone colorants: the impact of crystal packing. Dye Pigment 2000;45:169–76.
[64] Fuentealba P, Contreras R. Fukui function in chemistry. In: Sen KD, Parr RG, editors. Reviews of modern quantum chemistry a celebration of the contributions of Robert G Parr. Singapore: World Scientific Publishing Co.; 2002. pp. 1013–53.
[65] Fuentealba P, Florez E, Tiznado W. Topological analysis of the Fukui function. J Chem Theory Comput 2010;6:1470–8.
[66] Demchenko AP. The concept of λ-ratiometry in fluorescence sensing and imaging. J Fluoresc 2010;20:1099–128.
[67] Coropceanu V, André JM, Malagoli M, Brédas JL. The role of vibronic interactions on intramolecular and intermolecular electron transfer in p-conjugated oligomers. Theor Chem Acc 2003;110:59–69.
[68] Park YH, Kim Y-H, Kwon SK, Koo IS, Yang K. Theoretical studies on dicyanoanthracenes as organic semiconductor materials: reorganization energy. Bull Korean Chem Soc 2010;31:1649–56.
[69] Liu Y-L, Feng J-K, Ren A-M. Theoretical study of optical and electronic properties of the bis-dipolar diphenylamino-endcapped oligoarylfluorenes as promising light emitting materials. J Phys Org Chem 2007;20:600–9.
[70] Gupta N, Linschitz H. Hydrogen-bonding and protonation effects in electrochemistry of quinones in aprotic solvents. J Am Chem Soc 1997;119:6384–91.